Solid State Sciences 132 (2022) 106994

Contents lists available at ScienceDirect

Solid State Sciences

journal homepage: www.elsevier.com/locate/ssscie

Preparation, characterizations, dielectric properties and nonlinear behavior of $(Na^{+}_{1/3}Ca^{2+}_{1/3}Yb^{3+}_{1/3})Cu_3Ti_4O_{12}$ ceramics

Jutapol Jumpatam [a,*], Jakkree Boonlakhorn [b], Bundit Putasaeng [c], Narong Chanlek [d], Prasit Thongbai [e]

[a] Department of Fundamental Science, Faculty of Science and Technology, Surindra Rajabhat University, Surin, 32000, Thailand
[b] Department of Basic Science and Mathematics, Faculty of Science, Thaksin University, Songkhla Campus, Songkhla, 90000, Thailand
[c] National Metal and Materials Technology Center, National Science and Technology Development Agency, Thailand Science Park, Pathum Thani, 12120, Thailand
[d] Synchrotron Light Research Institute (Public Organization), 111 University Avenue, Maung District, Nakhon Ratchasima, 30000, Thailand
[e] Giant Dielectric and Computational Design Research Group (GD–CDR), Department of Physics, Faculty of Science, Khon Kaen University, Khon Kaen, 40002, Thailand

ARTICLE INFO

Keywords:
Scanning electron microscopy
Dielectric constant
Dielectric loss tangent
Nonlinear characteristics

ABSTRACT

We present the investigation of phase formation, microstructural, dielectric properties and nonlinear behaviors of $(Na_{1/3}Ca_{1/3}Yb_{1/3})Cu_3Ti_4O_{12}$ ceramics prepared by a modified sol-gel method under various sintering conditions. According to the Rietveld refinement analysis, the main phase $CaCu_3Ti_4O_{12}$-like $(Na_{1/3}Ca_{1/3}Yb_{1/3})Cu_3Ti_4O_{12}$ structure with a lattice constant of ≈7.384 Å was observed in the studied samples. The surface microstructural changes for the ceramics at different conditions were examined by scanning electron microscopy. The dielectric response and nonlinear behaviors of the specimens were methodically explored. At 1 kHz, a high dielectric constant of 5.49×10^3 with a low dielectric loss tangent ≈0.075 was successfully achieved. The sintered $(Na_{1/3}Ca_{1/3}Yb_{1/3})Cu_3Ti_4O_{12}$ ceramics exhibited good nonlinear behavior. The interfacial polarization at the grain boundaries based on the internal barrier layer capacitor structure could explain the dielectric behavior of the studied specimens. From the results of the X-ray photoelectron spectroscopy (XPS) analysis, the presence of Cu^{+}, Cu^{2+}, and Ti^{3+} ions might be the major cause of the n-type semiconductor nature inside the grains.

1. Introduction

The increasing performance of multilayer ceramic capacitors on giant dielectric compounds has been extensively investigated because of the massive demand for their applications in microelectronic industries. It is well known that a low dielectric loss tangent (tanδ) and large dielectric constant (ε′) over the temperature range of dielectric materials are highly desirable for industrial capacitor applications [1–19]. Over the past years, many studies have been investigated on the giant dielectric properties of perovskite-like $ACu_3Ti_4O_{12}$ (*A*CTO) compounds. $CaCu_3Ti_4O_{12}$ (CCTO), an interesting member of the family of materials, exhibits a very large ε′ value of approximately 10^4 over a broad temperature range with no phase transition [4]. Despite no clear explanation of the original cause of giant dielectric behaviors in *A*CTO-based materials, it is widely accepted that the grains and grain boundaries (GBs) of CCTO polycrystalline ceramics are semiconducting and insulating phases, respectively [10,20–22]. This electrically heterogeneous microstructure model is khown as an internal barrier layer capacitor (IBLC) structure. In contrast, intrinsic effects (i.e., mixed valence, structural frustration, and electron hopping) of the crystal structure cannot be overpassed [12]. Although giant dielectric behavior has been observed in CCTO polycrystalline ceramics, the high dielectric loss value limits their application limited [12,13,15,21,22]. Moreover, CCTO and *A*CTO-related ceramics display nonlinear current density (*J*) – electric field strength (*E*) properties, which make them desirable for varistor applications [10,16,23]. This extra behavior is resulted from the existence of an internal potential barrier along the GBs, which is the main source of the nonlinear behavior in their *A*CTO-related ceramics [10].

The $ACu_3Ti_4O_{12}$-family members, where $A = Y_{2/3}$, $Sm_{1/2}Na_{1/2}$, $Y_{1/2}Na_{1/2}$, $La_{1/2}Na_{1/2}$, and $Na_{1/3}Ca_{1/3}Y_{1/3}$, have also been confirmed to exhibit high ε′ values at room temperature (RT), similar to CCTO ceramics [4–7,23–28]. The mechanism to interpret the nature for the unusual dielectric phenomenon of these polycrystalline materials is widely described as the stronger IBLC effect. According to the $ACu_3Ti_4O_{12}$ family, some members exhibit interesting dielectric and nonlinear properties. For example, a high ε′ of 8.7×10^3 with low tanδ

* Corresponding author.
E-mail address: jutapol.j@srru.ac.th (J. Jumpatam).

https://doi.org/10.1016/j.solidstatesciences.2022.106994
Received 7 June 2022; Received in revised form 5 August 2022; Accepted 8 August 2022
Available online 13 August 2022

values of 0.07 at 1 kHz and RT can be obtained in $Na_{1/2}La_{1/2}Cu_3Ti_4O_{12}$ ceramics [26]. The sintered $Y_{2/3}Cu_3Ti_4O_{12}$ ceramics exhibited a low tanδ of 0.033 and a large ε′ with good temperature stability [27]. The excellent dielectric properties of $[Na_{1/3}Ca_{1/3}Lm^{3+}_{1/3}]$-$Cu_3Ti_4O_{12}$, where the Lm^{3+} ions were Y^{3+} and Bi^{3+}, were successfully obtained. For the $(Na_{1/3}Ca_{1/3}Bi_{1/3})Cu_3Ti_4O_{12}$ ceramics, a low tanδ value of ≈0.04 and an ε′ value higher than 10^4 were obtained at RT and 1 kHz. In addition, it exhibits good nonlinear *J-E* properties [25].

To optimize the high dielectric performance of CCTO-based ceramics, one of the investigations during the last decade has been to study the preparation processes. Conventional mixed-oxide or solid-state reaction methods are typically used to synthesize *A*CTO-related ceramics [11–14]. However, mythology requires repetitive grinding and firing at high temperatures (≈1050 °C) and long reaction times to eliminate the possible impurity phases. In contrast, the dielectric response can be significantly improved using chemical methods to synthesize CCTO-related compounds [9,18,19,29–31]. One of the most effective chemical methods is the sol-gel method, which is used to produce nanocrystalline CCTO-based compounds. Although many researcher groups mainly focused on the improvement of the dielectric properties in CCTO-based ceramics obtained by optimizing the doping or substituted modification or controlling preparation process, the reports in the effect of the modified substitution with mixed valence states in the A–sites for the CCTO structure combined with the controlled chemical solution for synthesis A-ternary CCTO-type $\left(Lx^{+}_{1/3}Ln^{2+}_{1/3}Lm^{3+}_{1/3}\right)Cu_3Ti_4O_{12}$ materials on the dielectric properties and nonlinear behaviors to seek the new giant dielectric materials have seldom been investigated systematically. Thus, quantification of this concept is important and constituted the main objective of the present work.

It was reported that the substituted Yb^{3+} ions in the CCTO ceramics prepared by a modified sol-gel method have greatly impacted on the dielectric properties and electric response. The reduction in tanδ for the CCTO ceramics were obtained with the Yb^{3+} substitution. The average grain size of CCTO ceramics were reduced by increasing with Yb^{3+} doping concentration. The microstructural changes had a slight impact on the dramatic increase observed in resistance at GBs (R_{gb}) of Yb-doped CCTO ceramics. It can be described that the increase in R_{gb} related to reduced tanδ may be caused by enhancing the electrostatic potential height at the GBs [32]. According to our previous work, high ε′ values ($>10^4$) with tanδ values below 0.1 at 10^3 Hz were successfully obtained in $Na_{1/3}Ca_{1/3}Y_{1/3}Cu_3Ti_4O_{12}$ ceramics prepared by the simple sol-gel method. The results found that ε′ increased with increasing average grain size with increasing sintering time based on the IBLC effect. In addition, the intrinsic properties (e.g. Schottky barrier) at the GBs related to R_{gb} value for the $Na_{1/3}Ca_{1/3}Y_{1/3}Cu_3Ti_4O_{12}$ ceramics were enhanced, giving rise to the decreased dielectric loss values [24]. Hence, a study on the grain size control by sintering process in the mixed three-valence states (Lx^{+}, Ln^{2+} and Lm^{3+} ions) into A-site in the *A*CTO lattice structure is still interesting and will provide a possible way to seek the new isostructural CCTO-type dielectric materials, showing giant dielectric properties and good nonlinear response. Therefore, from the previous concept, the aim of this research is to study the effect of the random distribution of Na^{+}, Ca^{2+} and Yb^{3+} ions in the A-site for the *A*CTO lattice, as the norminal formula of $Na^{+}_{1/3}Ca^{2+}_{1/3}Yb^{3+}_{1/3}Cu_3Ti_4O_{12}$ (NCYbCTO) metarials prepared by chemical method under the different preparation conditions on the structural, dielectric properties, electrical response and nonlinear behaviors. It is expected that a single phase NCYbCTO could be formed. Moreover, the improved dielectric properties and good nonlinear *J-E* behaviors of the ceramics by changing the intrinsic electrical properties at the GBs related to the dielectric loss could be accomplished as to the obtained in the $Na_{1/3}Ca_{1/3}Y_{1/3}Cu_3Ti_4O_{12}$ [24].

In this study, we used a simple thermal decompositon method to synthesize A-ternary CCTO-type NCYbCTO nanocrystalline powders. The effects of the preparation conditions on the structural, microstructural, dielectric, and nonlinear behaviors were systematically observed and discussed in detail. Densification of the ceramics showed that dense ceramic microstructures were obtained at a sintering temperature of 1075 °C. When the sintering temperature increased to 1100 °C, it was found that the sintered NCYbCTO ceramics decomposed and melted. Interestingly, the ε′ values were higher than 10^3, and the obtained low tanδ value was approximately 0.075 at 20 °C and 1 kHz. Good nonohmic behaviors were obtained for the sintered NCYbCTO ceramic samples. Impedance spectroscopy technique was employed to study the electrical responses of the grain and GB. The possible nature of this dielectric phenomenon is discussed in detail.

2. Experimental details

A fine NCYbCTO powder was synthesized by a simple thermal decomposition process using sodium acetate ($NaCH_3COO$), calcium acetate ($Ca(C_2H_3CO_2)_2{\cdot}H_2O$, yttertium acetate ($(CH_3CO_2)_3Yb{\cdot}H_2O$), copper acetate ($Cu(CH_3COO)_2{\cdot}H_2O$), $C_{16}H_{28}O_6Ti$ (75 wt% in isopropanol), deionized water, ethanol, citric acid, and ethylene glycol as raw starting materials. Details of the preparation process are described elsewhere [24]. Then, the obtained precursor was calcined at 850 °C for 8 h to form a substrate powder. The calcined powder was carefully ground and sifted to obtain fine NCYbCRTO powder. Subsequently, the resulting powder was cold-pressed into disks (diameter ≈9.8 mm and thickness ≈2.0 mm). The studied sintering conditions for the NCYbCTO green-body disks in this experimental were 1075 °C for 6 and 12 h (identified as the NCYb-S6 and NCYb-S12 samples, respectively).

X-ray diffraction (XRD; PANalytical, EMPYREAN) was used to determine the crystalline phase structure of the ceramic samples. The phase compositions and lattice parameters were refined using the Rietveld refinement technique. Transmission electron microscopy (TEM; Eindhoven) with energy-dispersive X-ray analysis (EDS) was used to determine the particle size and shape and to analyze the chemical composition of the calcined NCYbCTO powder. Desktop scanning electron microscopy (SEM; SEC, SNE4500 M) was employed to examine surface morforlogies of the ceramics. X-ray photoelectron spectroscopy (XPS; PHI5000 VersaProbe II, ULVAC−PHI) was performed to study the oxidation states of the transition metals in the sintered ceramic. The obtained XPS data were analyzed using the MultiPak software packaged by ULVAC-PHI, Inc.

For the dielectric and electrical measurements, details of the sample preparation were explained in our previous work [23]. A KEYSIGHT E4990A impedance analyzer was used to study the complex impedances and dielectric electrical properties. The measurement conditions in this work were measured over temperature and frequency ranges of −60−200 °C and 10^2−10^7 Hz, respectively. The nonlinear *J–E* behaviors at room temperature (RT) in silicone oil bath were studied (Keithley Model 247). The calculated nonlinear parameters have been described elsewhere [23].

3. Results and discussion

The crystalline phase composition of $(Na^{+}_{1/3}Ca^{2+}_{1/3}Yb^{3+}_{1/3})Cu_3Ti_4O_{12}$ specimens were investigated. The X-ray diffraction patterns for NCYbCTO ceramics are displayed in Fig. 1. The major CCTO phase (a body-centered cubic (BCC) structure, JCPDS No. 75–2188) was detected in both samples [4,6,8]. This observation is similar to that reported for $Na_{1/3}Ca_{1/3}Y_{1/3}Cu_3Ti_4O_{12}$ ceramics [23]. It is worth noting that, a small amount of secondary phase (CuO), corresponding to that the 2θ peak at approximately 35° is also existed in both ceramics. The experimental XRD patterns of the sintered NCYbCTO ceramics fitted by the Rietveld refinement method are illustrated in Fig. 1(b)-1(c), confirming the existence of a main phase of NCYbCTO, which is structured like CCTO. Corresponding to the Rietveld refinement profile fit, the quality data of the lattice constant (*a*), residual profile (R_p), expected (R_{exp}), and weighted profiles (R_{wp}), as well as the goodness of fit (GOF) values, were

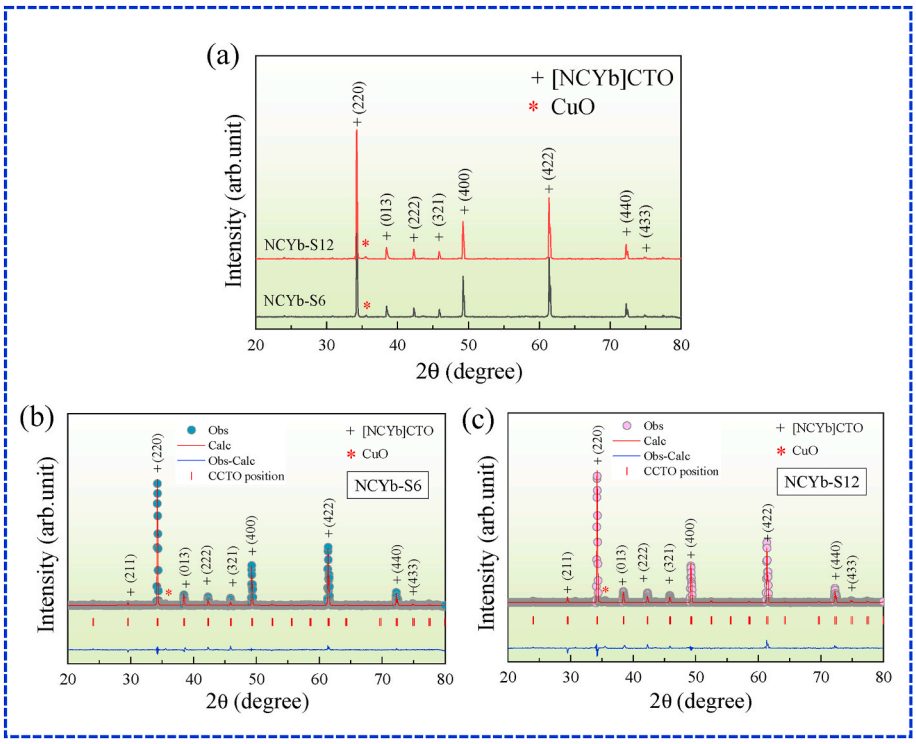

Fig. 1. (a) XRD patterns of the $(Na_{1/3}Ca_{1/3}Yb_{1/3})Cu_3Ti_4O_{12}$ ceramics sintered at 1075 °C for 6 and 12 h. Rietveld refinement profiles fitted for the (b) NCYb-S6 and (c) NCYb-S12 ceramics.

quantified and are listed in Table 1. The factor values of R_{exp}, R_p, and R_w for the ceramic samples were lower than 10%. The GOF values were approximately 2–4%. The *a* values of the C1–S6 and C1–S12 ceramic samples were 7.385(5) and 7.383(2) Å, respectively. These values are between the corresponding values for $Na_{1/2}Yb_{1/2}Cu_3Ti_4O_{12}$ (7.361 Å) and CCTO (7.391 Å) [4]. It is because a Ca^{2+} ion (r_6 = 0.99 Å) of the CCTO structure is larger than that of the mean Na^+ (r_6 = 0.95 Å) and Yb^{3+} (r_6 = 0.86 Å) ions in the $Na_{1/2}Yb_{1/2}Cu_3Ti_4O_{12}$ [33]. There were the randomly distribution of Na^+, Yb^{3+}, and Ca^{2+} ions at the A-site of crystal. The enlarged *a* values for the NCYbCTO structure may be due to the partial replacement of Na^+ and Yb^{3+} ions in the $Na_{1/2}Yb_{1/2}Cu_3Ti_4O_{12}$ structure by Ca^{2+} ions. It is found that the *a* values of NCYbCTO ceramics are slightly lower than that observed in $Na_{1/3}Ca_{1/3}Y_{1/2}Cu_3Ti_4O_{12}$ ceramics prepared by the solid state reaction and the chemical methods [23,24], whereas the values are largely lower than that obtained in $Na_{1/3}Ca_{1/3}Bi_{1/2}Cu_3Ti_4O_{12}$ ceramics [25]. These may be due to the difference in the ionic radii of the A-sites of the crystal lattice. Considering the ionic radii for only Lm^{3+} charge ions, it was observed that Yb^{3+} ion is smaller than those of both Y^{3+} (r_6 = 0.93 Å) and Bi^{3+} (r_6 = 1.03 Å) ions [33] (see Table 2).

Fig. 2(a) shows the EDS spectra of the NCYbCTO powder. It is clearly seen that the main elemental elements, Na, Ca, Yb, Cu, Ti, and O, were detected. As shown in the inset of Fig. 2(a), the particle size of the calcined powder is approximately 180–400 nm. To study the surface microstructure for the NCYbCTO ceramics sintered at 1075 °C, as revealed in Fig. 2(b)–(c), it was found that the sintering conditions had a significant impact on the microstructure. The results showed that the average grain size of the sintered NCYbCTO ceramics at 1075 °C increased slightly as the holding time increased from 6 to 12 h. The change in the grain size of the ceramics may be due to the liquid-phase sintering mechanism, as observed in CCTO-related ceramics [11,24,34–36]. This mechanism is reasonable since the eutectic temperature of $CuO–TiO_2$ is approximately 919 °C [13,37,38]. The detected CuO-rich phase with irregular shape along the grain boundaries for the NCYbCTO ceramics is observed as the same occurred in the $Na_{1/3}Ca_{1/3}Y_{1/3}Cu_3Ti_4O_{12}$ ceramics [24]. The observed secondary phase in the NCYbCTO ceracmics might also be owing to the large disparity of Yb^{3+} ion compared with the Na^+ and Ca^{2+} ions, leading to the large distortions of the *A*CTO lattice, possibly causing Cu segregation along the GBs.

Fig. 3 displays the ε′ and tanδ as a function of frequencies for the NCYbCTO samples at 20 °C. The giant ε′ value of all ceramics was almost independent of the frequency over the frequency range of 10^2–10^6 Hz. A rapid drop in ε′ the values at 10^5 Hz for the ceramic samples is clearly observed, which is consistent with the observed strong increase in tanδ

Table 2
Lattice parameter (a) and structural data obtained from the Rietveld refinement profile fits of the $(Na_{1/3}Ca_{1/3}Yb_{1/3})Cu_3Ti_4O_{12}$ samples sintered at 1075 °C for 6 and 12 h.

Ceramic	*a* (Å)	R_{exp} (%)	R_p (%)	R_w (%)	GOF
NCYb-S6	7.385(5)	5.161	5.910	8.790	2.901
NCYb-S12	7.383(2)	4.262	5.047	8.531	4.007

Table 1
Dielectric constant (ε′) and loss tangent (tanδ) at 20 °C and 1 kHz, the activation energy for dielectric relaxation (E_a), for dc conduction (E_{cond}) and for conduction at grain (E_g) and at grain boundaries (E_{gb}), non-Ohmic properties (α and E_b values) at RT for NCYbCTO samples sintered at 1075 °C for 6 and 12 h.

Sample	ε′	tanδ	E_a (eV)	E_{cond} (eV)	E_g (eV)	E_{gb} (eV)	α	E_b (V/cm)
NCYb-S6	5095	0.076	0.145	0.661	0.125	0.654	4.83	3591
NCYb-S12	5488	0.075	0.122	0.639	0.106	0.649	4.92	3559

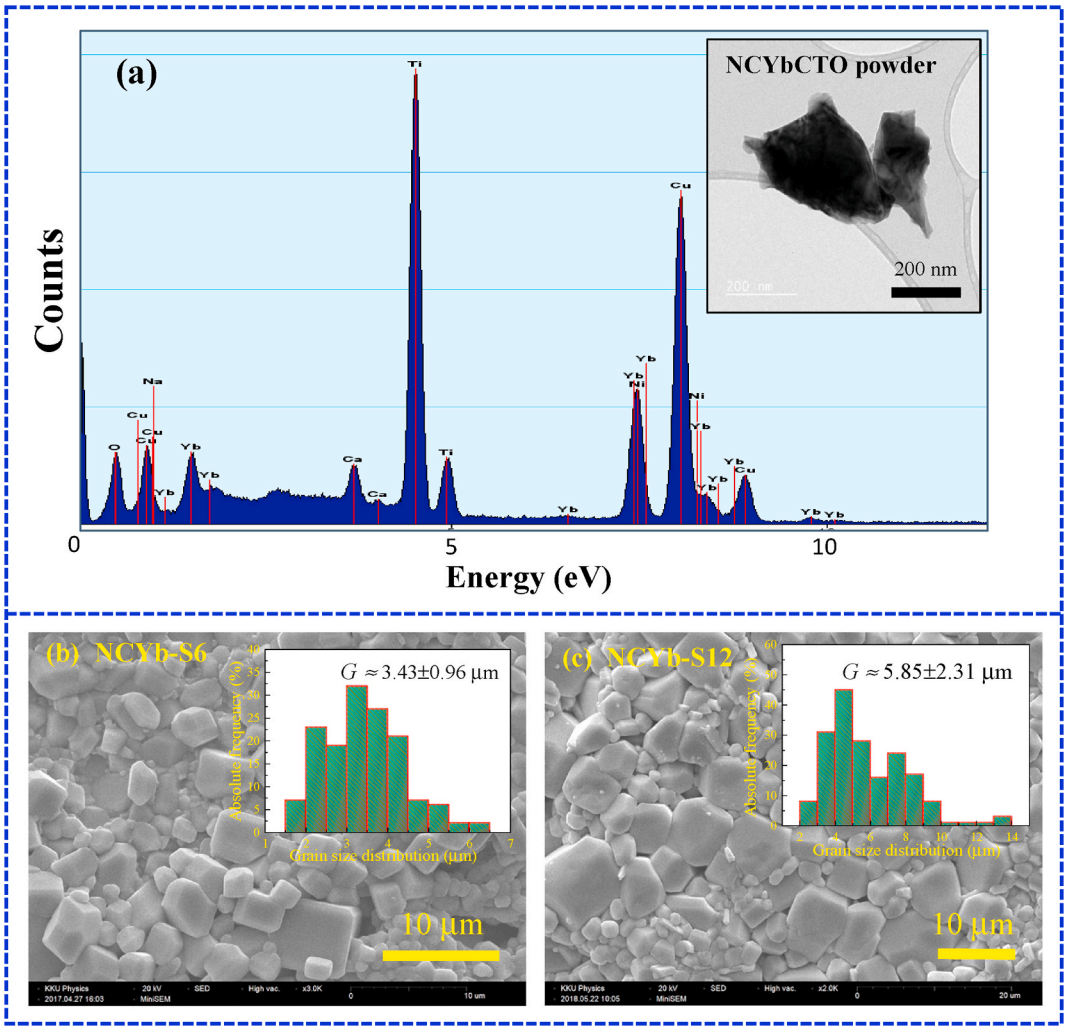

Fig. 2. (a) EDS spectra of the NCYbCTO powder; inset shows TEM image of morphology of the NCYbCTO powder. The SEM images of the surfaces revealing the morphologies of (b) NCYb-S6 and (c) NCYb-S2 ceramic samples.

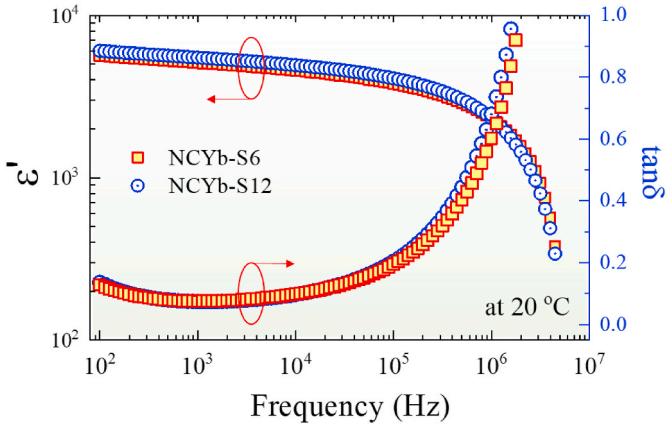

Fig. 3. Frequency dependence of ε′ and tanδ at 20 °C for the $(Na_{1/3}Ca_{1/3}Yb_{1/3})Cu_3Ti_4O_{12}$ ceramics sintered at 1075 °C for 6 and 12 h.

values at high frequencies. This behavior is khown as the primary dielectric relaxation mechanism, and is similar to that reported for CCTO-related ceramics [4,13,15,20]. The values of ε′ at 1 kHz and 20 °C for NCYb-S6 and NCYb-S12 were 5095 and 5488, respectively. According to the space charge polarization model based on the IBLC effect at the GBs mechanism, the dielectric response results of the NCYbCTO ceramics are likely associated with the average grain size, as observed in the SEM images in Fig. 2(b)–(c). The changed dielectric response is consistent with a change in microstructure, according to the IBLC structure model. This result is similar to observed in the previous work [24]. The tan δ values for the NCYb-S6 and NCYb-S12 samples were almost the same and were found to be approximately 0.075 at 1 kHz. The ε′ and tanδ values at 1 kHz and 20 °C for all ceramic samples are summarized in Table 1. The overall dielectric behavior as a function of frequency dependence in the NCYbCTO ceramics was similar to that observed for the ACTO family compounds [23,27,28]. Note that the enhanced dielectric properties may be optimized by varying the preparation conditions (sintering temperature and/or sintering time). Nevertheless, this determination is outside the scope of this work.

To study the dielectric electrical properties of the NCYbCTO ceramics, the dielectric relaxation behavior was studied by considering the frequency dependence of real part ε′ and imaginary part ε″ ($\varepsilon'' = \varepsilon' \times \tan\delta$) at different temperatures, as illustrated in Fig. 4 ε′ and ε″ *vs.* frequency for the NCYb-S6 and NCYb-S12 ceramics were plotted in the temperature range from −50 to 150 °C. It is noteworthy that a stepped ε′ reduction shifts to higher frequencies as the temperature increases. This behavior is khown as the thermally activated dielectric relaxation effect [6,27,39,40]. Three parts of the dielectric response were observed, as reported by Li et al. [39]. The source of the high ε′, exhibited at high temperature, in the low-frequency range might be caused by a

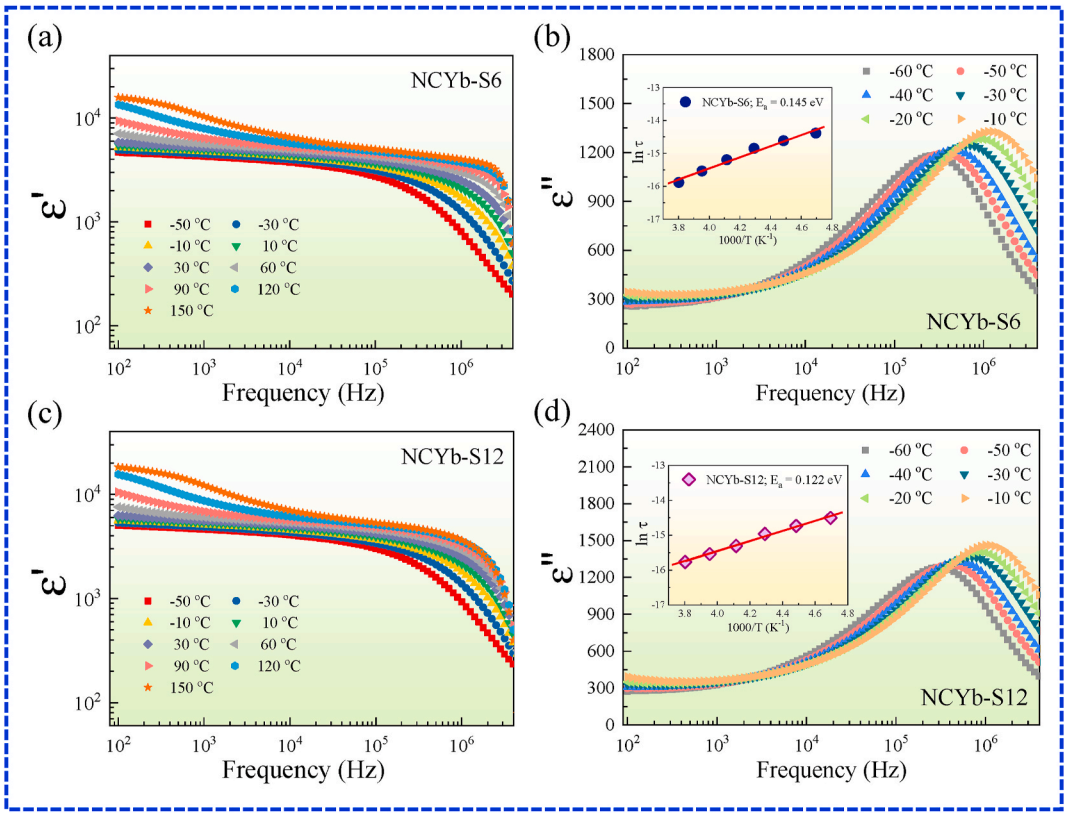

Fig. 4. Frequency dependence of (a)–(c) ε′ and (b)–(d) ε″ at different temperatures for $(Na_{1/3}Ca_{1/3}Yb_{1/3})Cu_3Ti_4O_{12}$ samples. Insets of (b) and (d) show Arrhenius plots for the temperature dependence of τ for the NCYb-S6 and NCYb-S12 samples, respectively.

sample-electrode interface response [39], while the high frequency ε' originates from the electrical response inside grains or bulk response [20]. The observed primary plateau ε at intermediate frequencies is attributed to the dielectric behavior of GBs [4,26,28,41]. This dielectric behavior is typically observed in CCTO-and ACTO-related ceramics. As shown in Fig. 4(b) and (d). The relaxation peaks of ε'' shifted to high frequencies as the temperature increased, corresponding to a rapid decrease in ε'. Using the dielectric relaxation results, the dielectric relaxation times (τ) at various temperatures were obtained and can also be calculated using the relations $\omega\tau = 1$ and $\omega = 2\pi f_{peak}$, where f_{peak} is the response frequency corresponding to the peak of ε''. The temperature variation of the τ values follows Arrhenius's law:

$$\tau = \tau_0 \exp\left(\frac{U}{k_B T}\right), \quad (1)$$

where U is the activation energy required for thermal relaxation, τ_0 is the pre-exponential factor, k_B is Boltzmann's constant, and T is the absolute temperature. As illustrated in Fig. 4(b) and (d), the good linear τ values were fitted by Eq. (1). From the fitting results, the calculated activation energies of the dielectric relaxations were found to be 0.145 and 0.122 eV for the NCYb-S6 and NCYb-S12 ceramics, respectively, which are comparable to those reported for CCTO (0.093 eV), $Na_{1/2}Y_{1/2}Cu_3Ti_4O_{12}$ (0.112 eV), $Y_{2/3}Cu_3Ti_4O_{12}$ (0.112–0.0123 eV), and $Na_{1/3}Ca_{1/3}Bi_{1/3}Cu_3Ti_4O_{12}$ ceramics (0.112–0.121 eV). These activation energies are related to the bulk response of the ceramics.

Fig. 5 displays the ε' at 1 kHz as a function of temperatures for the NCYbCTO samples. The high ε' values in the order of 10^3 are relatively stable over a wide temperature range of -60 - 100 °C. It is worth noting that ε' increased with increasing temperature at 50 °C, corresponding to an increase in tanδ values (inset of Fig. 5). The behavior of high-temperature range for both samples was a result of the direct current conductivity of delocalized charges in the bulk, as observed for CCTO

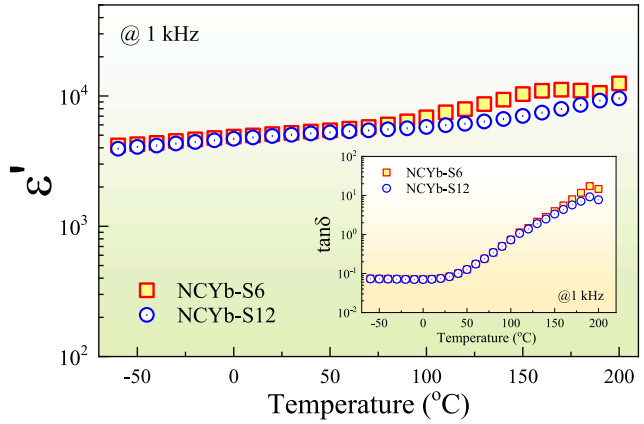

Fig. 5. Temperature dependence of ε′ and tanδ (inset) at 1 kHz for the $(Na_{1/3}Ca_{1/3}Yb_{1/3})Cu_3Ti_4O_{12}$ samples sintered at 1075 °C for 6 and 12 h.

ceramics and other related materials [6,35,42].

In accordance with the IBLC structure for ACTO polycrystalline ceramics, an ideal equivalent circuit consisting of two parallel resistor-capacitor (R–C) elements connected in series was proposed, one RC element for the grain part (consisting of the grain resistance (R_g) and the capacitance of the grains (C_g)) and the another for the GB part (consisting of the GB resistance (R_{gb}) and capacitance of GBs (C_{gb})) [20]. Impedance spectroscopy analysis is often used to study the electrically heterogeneous microstructure of electroceramics [20,36,39,43,44]. The impedance data for the samples were calculated after the sample geometry by considering the ratio of the area of the electrode/pellet thickness. To investigate the nature of the GBs, as shown in Fig. 6(a), the values of R_{gb} at any temperature were evaluated by fitting complex

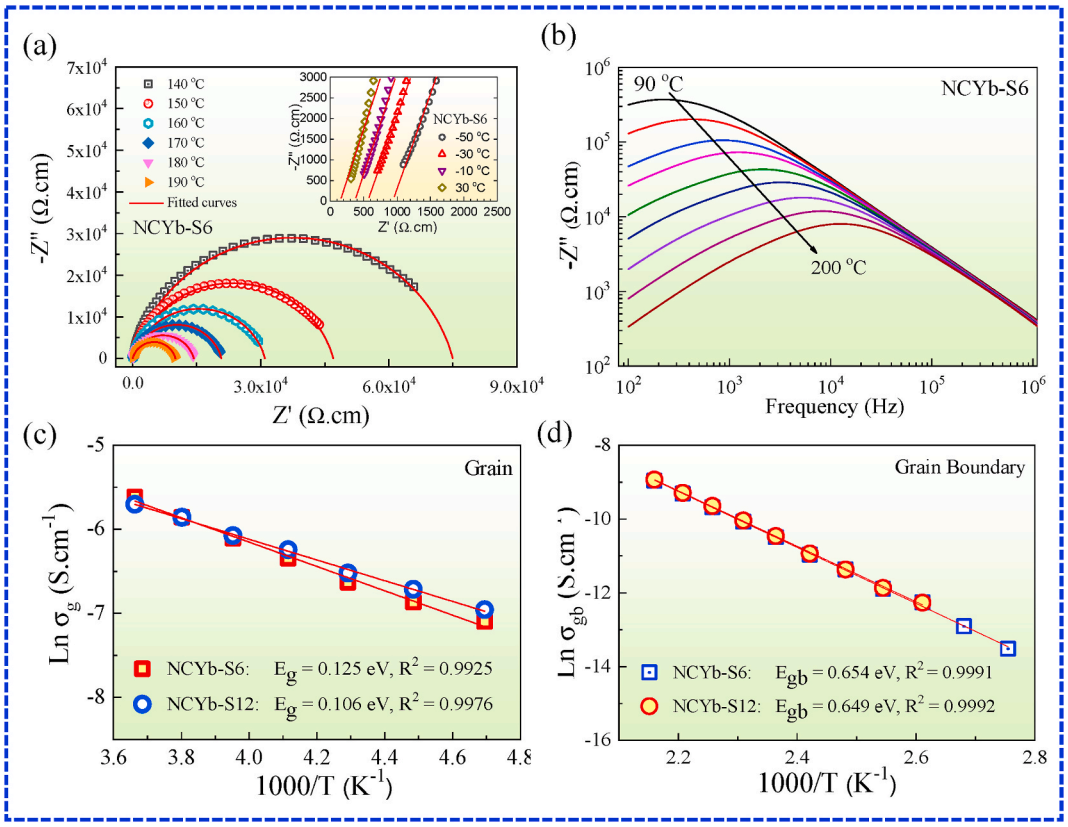

Fig. 6. (a) Impedance complex plane plots in the temperature range of 150–190 °C for the NCYb-S6 sample; red solid curves are the fitted data using Eq. (2). Inset of (a) show an expanded view of the high–frequency data close to the origin in the temperature range from −50 to 30 °C; red solid lines are the eye guidelines for estimating R_g (b) Frequency dependence of -Z″ for the NCYb-S6 sample at various temperature from 90 °C to 190 °C. Arrhenius plots of (c) grain conductivity (σ_g) and (d) GB conductivity (σ_{gb}) of the NCYbCTO samples. (For interpretation of the references to colour in this figure legend, the reader is referred to the Web version of this article.)

impedance (Z*) data in temperature range of 140–190 °C of the NCYb-S6 sample using a modified equation corresponding to the equivalent circuit of the modified equation for a Z* plot as follows [6]:

$$Z^* = R_g + \frac{R_{gb}}{1 + (i\omega R_{gb} C_{gb})^{\alpha}}, \quad (2)$$

where α is a constant value ($0 < \alpha \leq 1$) and C_g and C_{gb} are the capacitances of the grains and GBs, respectively. C_g is inaccessible, and the capacitor can be ignored from the circuit. As shown in Fig. 6(a), the diameter of the semicircle arcs and the nonzero intercept of the NCYb-S6 sample decreased with increasing temperature, indicating that a thermal activation process occurred at the GBs, corresponding to a reduction in R_{gb}. Concurrently, R_g tended to decrease with increasing temperature, as estimated by the eye-red guidelines (inset of Fig. 6(a)), confirming the semiconducting nature of the grains in the sample. It is clear that the NCYbCTO ceramics are electrically heterogeneous, consisting of an insulating part of the GB layers sandwiched by semiconducting grains. Therefore, it is reasonable to suggest that the high ε′ values of the NCYbCTO ceramics were likely caused by interfacial polarization at the GBs. This behavior is usually observed to describe the colossal dielectric behavior in CCTO and $ACu_3Ti_4O_{12}$ ceramics [23,40,45].

To optimize the results, we also studied the frequency dependence of -Z″ measured in the temperature range of 90–200 °C for the C1–S6 ceramic, as illustrated in Fig. 6. The apparent maximum values of Z″ change to higher frequencies with increasing temperature, which indicates a thermal excitation process at the GBs. The apparent Z″ is consistent with a large semicircular arc [Fig. 6(a)] and represents the electrical response of the GB. Using the relationship between R_{gb} and Z″, R_{gb} at various temperatures can be calculated from the maximum Z″ peak, $Z''_{max} = R_{gb}/2$. The activation energy required for the conduction of charge carriers in the grains (E_g) and GB region (E_{gb}) can be calculated using the derived Arrhenius law:

$$\ln \sigma_{g/gb} = \left(\frac{-E_{g/gb}}{k_B T}\right) + \ln \sigma_0 \quad (3)$$

where $\sigma_{g/gb} = 1/R_{g/gb}$, σ_0 is the pre-exponential term, T is the absolute temperature (K), k_B is the Boltzmann constant, and E_g and E_{gb} are the grain and GB activation energies of the grain and grain boundaries, respectively. As shown in Fig. 6(c) and (d), the experimental data were fitted using Eq. (3). For the fitted curves, the diameter of the solid line curve was adjusted by tuning the R_{gb} parameter and did not depend on the C_{gb} values. The E_g and E_{gb} values for all the ceramic samples were obtained from the slopes of the plots. The calculated E_g values of the NCYb-S6 and NCYb-S12 ceramics were 0.125 and 0.106 eV, respectively, while the calculated E_{gb} values were 0.654 and 0.648 eV, respectively (summarized in Table 1). The obtained E_g and E_{gb} values were nearly the same as those reported for CCTO and related $ACu_3Ti_4O_{12}$ ceramics [23,26,36]. The large difference of E_g and E_{gb} values indicates the formation of an IBLC structure, which is an important cause of the dielectric response observed in CCTO-type materials. Considering the electrical response at the GBs, it was found that the E_{gb} values of the NCYbCTO ceramics are lower than that the values of 0.677–0.797 eV observed in $Na_{1/3}Ca_{1/3}Y_{1/3}Cu_3Ti_4O_{12}$ ceramics [23,24]. In meanwhile, the values are higher than the observed in $Na_{1/3}Ca_{1/3}Bi_{1/3}Cu_3Ti_4O_{12}$ ceramics [25]. It is indicated that the containing Yb_2O_3 concentration in the *A*CTO structure might play a significant role for changing intrinsic properties (e.g. Schottky barrier) at the GBs. Therefore, these results confirmed that the microstructure of the NCYbCTO

ceramics was electrically heterogeneous, and the dielectric response could be attributed to interfacial polarization based on the IBLC model. However, the intrinsic origin of the mixed valence states of Cu^{+} and Ti^{3+} and/or the point defects inside the grains cannot be ignored and absurdly excluded [46].

In addition to the study of the electrical response of the NCYbCTO ceramics using impedance analysis, this behavior was also studied using the alternating current (AC) conductivity (σ_{ac}) as a function of temperature. As shown in Fig. 7, the temperature dependence of the σ_{ac} values over the frequency range of 10^{2}–10^{6} Hz was investigated for the selected NCYb-S6 ceramic. It was found that the values of σ_{ac} in the low-frequency range almost saturate at a constant value, which is close to the direct current (dc) conductivity (σ_{dc}). This result indicates that the electric field does not affect the hopping conduction mechanism at low frequencies. Therefore, σ_{ac} at 10^{2} Hz can be estimated from σ_{dc}. As shown in Fig. 7, σ_{dc} increased with increasing temperature. Arrhenius plots for both ceramics at different frequencies are shown in the inset of Fig. 7. The relationship between 1000/T and ln σ_{dc} divides the activation energy of the DC conductivity and follows the Arrhenius principle [47]:

$$\sigma_{dc} = \sigma_0 \exp\left(\frac{-E_{cond}}{k_B T}\right) \tag{4}$$

where E_{cond} is the activation energy required for the DC conduction. The E_{cond} values were calculated to be 0.661 and 0.639 eV for the NCYb-S6 and NCYb-S12 samples, respectively. These values were close to the E_{gb} values. This implies that the DC conduction process is closely associated with the electrical response of the GBs. It is evident that the large dielectric behavior of the NCYbCTO ceramics arises from the IBLC model based on the interfacial polarization effect.

The nonlinear *J-E* behaviors at RT of the NCYbCTO ceramics under different preparation conditions were also studied, as shown in Fig. 8. It was observed that all ceramic samples exhibited nonlinear behavior. The α values were calculated using Eq. (1) and were found to be 4.83 and 4.92 for the NCYb-S6 and NCYb-S12 ceramics, respectively. The E_b values were 3591 V/cm and 3559 V/cm, respectively. Both the E_b and α values for all the samples are summarized in Table 1. The nonlinear *J-E* properties of all sintered NCYbCTO ceramic samples differed slightly. Values of α and E_b slightly increased when increasing sintering duration. This observed result is close to studied in the previous work [24]. The variation of E_b values are associated with the change of the R_{gb} in the *A*CTO-type ceramics, corresponding to the geometric (volume fraction

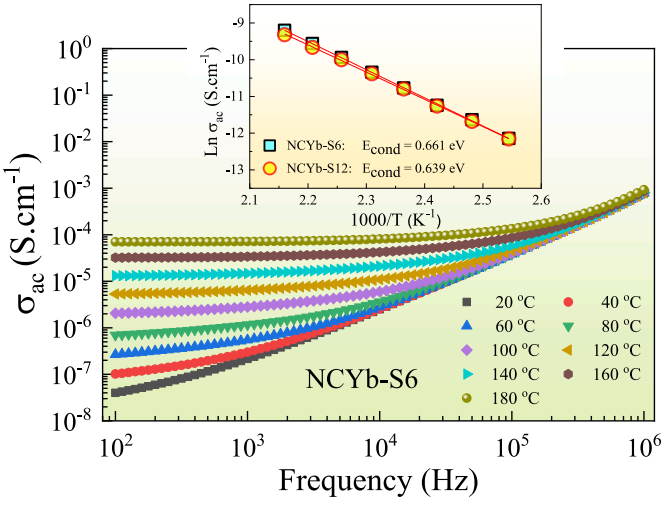

Fig. 7. Frequency dependence of σ_{ac} at various temperature for the NCYb-S6 samples; inset shows Arrhenius plot of dc conductivity (σ_{dc}) for the $Na_{1/3}Ca_{1/3}Yb_{1/3}Cu_3Ti_4O_{12}$ samples sintered at 1075 °C for 6 and 12 h.

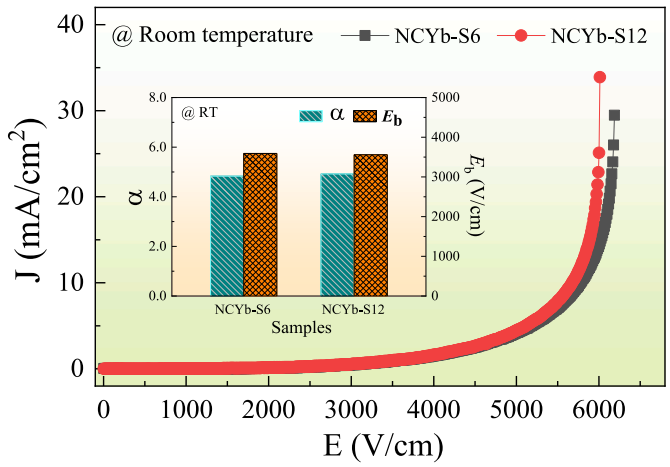

Fig. 8. Nonlinear (*J–E*) characteristics of the $Na_{1/3}Ca_{1/3}Yb_{1/3}Cu_3Ti_4O_{12}$ samples at room temperature; inset shows values of α and E_b.

of GBs) and intrinsic properties (E_{gb} and Φ_b) at GBs. In general, both the geometric and intrinsic properties of grain and GBs affect the nonlinear behvaios. It is worth noting that the variation in E_b was consistent with the number of grain boundary layers in the thickness of each ceramic. In this case, it was found that E_b of NCYbCTO ceramics slightly reduced as the average grain size increased. This indicates that the intrinsic properties of the GBs was dominant than the geometric, which is likely because of the different values of Φ_b at the GBs of the ceramics. This nonlinear response can be used in varistors to detect high-voltage transients entering the circuit of an electronic device. It has been accepted extensivley that the nonlinear *J-E* behavior of CCTO-based polycrystalline ceramics may be resulted from the presence of Schottky potential barriers at the GBs sandwiched between semiconducting grains based on the electrically heterogeneous IBLC structure.

To study the possible source of the electrical properties of the grains in the ceramics, XPS was employed to investigate the oxidation states of the polyvalent cations related to the *n*-type semiconducting grains in the bulk. Fig. 9 displays the XPS spectrum of the Cu*2p* region of the C1–S6 ceramic. The Cu*2p* region can be divided into three peaks using Gaussian-Lorentzian profile fitting. The highest XPS peak (≈933 eV) is attributed to the presence of Cu^{2+} in the NCYbCTO structure [25,41,46]. The smaller peaks at relatively lower (≈931 eV) and higher (≈935 eV) binding energies indicate the presence of Cu^{+} and Cu^{3+} ions, respectively [23–25]. The calculated ratios of Cu^{+}/Cu^{2+} and Cu^{3+}/Cu^{2+} for

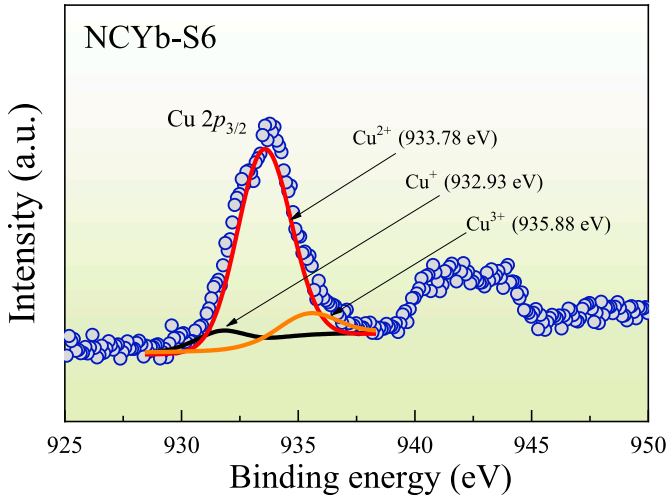

Fig. 9. XPS spectra for the Cu*2p* region for the NCYb-S6 sample.

the NCYbCTO ceramic were approximately 12.38% and 10.56%, respectively. Additionally, the ratio of Ti^{3+}/Ti^{4+} obtained from the XPS technique was calculated and found to be in close proximity. The presence of Cu^{+}, Cu^{3+}, and Ti^{3+} ions may affect the electrical semiconducting properties of the grains. Although the origin of semiconducting grains in NCYbCTO ceramics is very complex, it is likely that the conduction mechanism of the grains may be attributed to the charge carrier hopping processes in the NCYbCTO structure.

4. Conclusions

NCYbCTO ceramics were prepared by a simple thermal decomposition method under different sintering conditions. By optimizing the sintering conditions, the NCYbCTO ceramic exhibited a low tanδ of approximately 0.075 with high ε′ values of 5.8×10^3at 1 kHz and 20 °C. Nonlinear *J*−*E* behaviors were observed in the NCYbCTO ceramics and were found to be closely consistent with the microstructural changes. It was found that the ceramics had electrically heterogeneous microstructures confirmed by the impedance spectroscopy technique. The large dielectric response is likely caused by the strong interfacial polarization at the GBs. XPS was used to confirm the presence of Cu^{+}, Cu^{3+}, and Ti^{3+} ions. The presence of these ions may affect the electrical semiconducting properties of the grains. The dielectric behavior and nonlinear properties were described based on the IBLC effect.

Author statement

Jutapol Jumpatam: Conceptualization, Methodology, Data curation, Resources, Investigation, Validation, Visualization, Writing - Original Draft, Writing – review & editing, Funding acquisition, Project administration. **Jakkree Boonlakhorn:** Data curation, Investigation, Validation. **Bundit Putasaeng:** Formal analysis, Investigation, Resources. **Narong Chanlek:** Formal analysis, Investigation, Resources. **Prasit Thongbai:** Conceptualization, Data curation, Resources, Validation, Supervision.

Declaration of competing interest

The authors declare that they have no known competing financial interests or personal relationships that could have appeared to influence the work reported in this paper.

Acknowledgments

This work was financially supported by the Office of the Permanent Secretary, Ministry of Higher Education, Science, Research, and Innovation [Grant Number RGNS 63-209]. The authors thank the SUT-NANOTEC-SLRI Joint Research Facility for the XPS facility in Nakhon Ratchasima, Thailand. This work would like to thank the Faculty of Science and Technology at Surindra Rajabhat University.

References

[1] S. Krohns, P. Lunkenheimer, S. Meissner, A. Reller, B. Gleich, A. Rathgeber, T. Gaugler, H.U. Buhl, D.C. Sinclair, A. Loidl, The route to resource-efficient novel materials, Nat. Mater. 10 (2011) 899–901.

[2] W. Hu, Y. Liu, R.L. Withers, T.J. Frankcombe, L. Norén, A. Snashall, M. Kitchin, P. Smith, B. Gong, H. Chen, J. Schiemer, F. Brink, J. Wong-Leung, Electron-pinned defect-dipoles for high-performance colossal permittivity materials, Nat. Mater. 12 (2013) 821–826.

[3] C.C. Homes, T. Vogt, S.M. Shapiro, S. Wakimoto, A.P. Ramirez, Optical response of high-dielectric-constant perovskite-related oxide, Science 293 (2001) 673–676.

[4] M.A. Subramanian, D. Li, N. Duan, B.A. Reisner, A.W. Sleight, High dielectric constant in $ACu_3Ti_4O_{12}$ and $ACu_3Ti_3FeO_{12}$ phases, J. Solid State Chem. 151 (2000) 323–325.

[5] P. Liang, Y. Li, Y. Zhao, L. Wei, Z. Yang, Origin of giant permittivity and high-temperature dielectric anomaly behavior in $Na_{0.5}Y_{0.5}Cu_3Ti_4O_{12}$ ceramics, J. Appl. Phys. 113 (2013), 224102.

[6] J. Liu, C.G. Duan, W.N. Mei, R.W. Smith, J.R. Hardy, Dielectric properties and Maxwell-Wagner relaxation of compounds $ACu_3Ti_4O_{12}$ (A=Ca,$Bi_{2/3}$,$Y_{2/3}$,$La_{2/3}$), J. Appl. Phys. 98 (2005), 093703.

[7] J. Jumpatam, A. Mooltang, B. Putasaeng, P. Kidkhunthod, N. Chanlek, P. Thongbai, S. Maensiri, Effects of Mg^{2+} doping ions on giant dielectric properties and electrical responses of $Na_{1/2}Y_{1/2}Cu_3Ti_4O_{12}$ ceramics, Ceram. Int. 42 (2016) 16287–16295.

[8] G. Du, F. Wei, W. Li, N. Chen, Co-doping effects of A-site Y^{3+} and B-site Al^{3+} on the microstructures and dielectric properties of $CaCu_3Ti_4O_{12}$ ceramics, J. Eur. Ceram. Soc. 37 (2017) 4653–4659.

[9] K. Prompa, E. Swatsitang, T. Putjuso, Very low loss tangent and giant dielectric properties of $CaCu_3Ti_4O_{12}$ ceramics prepared by the sol–gel process, J. Mater. Sci. Mater. 28 (2017) 15033–15042.

[10] S.Y. Chung, I.D. Kim, S.J.L. Kang, Strong nonlinear current–voltage behaviour in perovskite-derivative calcium copper titanate, Nat. Mater. 3 (2004) 774–778.

[11] C.M. Wang, K.S. Kao, S.Y. Lin, Y.C. Chen, S.C. Weng, Processing and properties of $CaCu_3Ti_4O_{12}$ ceramics, J. Phys. Chem. Solid. 69 (2008) 608–610.

[12] L. Ni, X.M. Chen, X.Q. Liu, Structure and modified giant dielectric response in $CaCu_3(Ti_{1-x}Sn_x)_4O_{12}$ ceramics, Mater. Chem. Phys. 124 (2010) 982–986.

[13] P. Thongbai, J. Jumpatam, T. Yamwong, S. Maensiri, Effects of Ta^{5+} doping on microstructure evolution, dielectric properties and electrical response in $CaCu_3Ti_4O_{12}$ ceramics, J. Eur. Ceram. Soc. 32 (2012) 2423–2430.

[14] J. Zhang, Z. Li, S. Guo, W. Lu, Z. Chen, X. Guo, R. Hao, D. Wang, Z. Lei, L. Li, J. Song, The enhanced cutoff frequency of dielectric constant for K-doped $Na_{0.5}Y_{0.5}Cu_3Ti_4O_{12}$ ceramics, Mater. Chem. Phys. 277 (2022), 125500.

[15] J. Jumpatam, B. Putasaeng, T. Yamwong, P. Thongbai, S. Maensiri, Enhancement of giant dielectric response in Ga-doped $CaCu_3Ti_4O_{12}$ ceramics, Ceram. Int. 39 (2013) 1057–1064.

[16] J. Boonlakhorn, P. Thongbai, Enhanced non−Ohmic properties and giant dielectric response of (Sm+Zn) co−doped $CaCu_3Ti_4O_{12}$ ceramics, Ceram. Int. 43 (2017) 12736–12741.

[17] L. Singh, U.S. Rai, K.D. Mandal, A. Rai, Effect of processing routes on microstructure, electrical and dielectric behavior of Mg-doped $CaCu_3Ti_4O_{12}$ electro-ceramic, Appl. Phys. A 112 (2013) 891–900.

[18] D. Xu, K. He, R. Yu, X. Sun, Y. Yang, H. Xu, H. Yuan, J. Ma, High Dielectric Permittivity and Low Dielectric Loss in Sol–Gel Derived Zn Doped $CaCu_3Ti_4O_{12}$ Thin Films, vol. 153, 2015, pp. 229–235.

[19] M. Chinnathambi, A. Sakthisabarimoorthi, M. Jose, R. Robert, Study of the Electrical and Dielectric behaviour of selenium doped CCTO ceramics prepared by a facile sol-gel route Mater, Chem. Phys. 272 (2021), 124970.

[20] D.C. Sinclair, T.B. Adams, F.D. Morrison, A.R. West, $CaCu_3Ti_4O_{12}$: one-step internal barrier layer capacitor, Appl. Phys. Lett. 80 (2002) 2153.

[21] J.A. Cortés, H. Moreno, S. Orrego, V.D.N. Bezzon, M.A. Ramírez, Dielectric and non-ohmic analysis of Sr^{2+} influences on $CaCu_3Ti_4O_{12}$-based ceramic composites, Mater. Res. Bull. 134 (2021), 111071.

[22] J. Jumpatam, B. Putasaeng, N. Chanlek, J. Boonlakhorn, P. Thongbai, N. Phromviyo, P. Chindaprasirt, Significantly improving the giant dielectric properties of $CaCu_3Ti_4O_{12}$ ceramics by co-doping with Sr^{2+} and F^{-} ions Mater, Res. Bull. 133 (2021), 111043.

[23] J. Jumpatam, W. Somphan, B. Putasaeng, N. Chanlek, P. Kidkhunthod, P. Thongbai, S. Maensiri, Nonlinear electrical properties and giant dielectric response in $Na_{1/3}Ca_{1/3}Y_{1/3}Cu_3Ti_4O_{12}$ ceramic Mater, Res. Bull. 90 (2017) 8–14.

[24] J. Jumpatam, A. Moontang, B. Putasaeng, P. Kidkhunthod, N. Chanlek, P. Thongbai, Preparation, characterization, and dielectric properties of $CaCu_3Ti_4O_{12}$-related $(Na_{1/3}Ca_{1/3}Y_{1/3})Cu_3Ti_4O_{12}$ ceramics using a simple sol–gel method, J. Mater. Sci. Mater. 28 (2017) 14839–14847.

[25] P. Kum-onsa, P. Thongbai, B. Putasaeng, T. Yamwong, S. Maensiri, $Na_{1/3}Ca_{1/3}Bi_{1/3}Cu_3Ti_4O_{12}$: a new giant dielectric perovskite ceramic in $ACu_3Ti_4O_{12}$ compounds, J. Eur. Ceram. Soc. 35 (2015) 1441–1447.

[26] P. Thongbai, T. Yamwong, S. Maensiri, Dielectric properties and electrical response of grain boundary of $Na_{1/2}La_{1/2}Cu_3Ti_4O_{12}$ ceramics, Mater. Res. Bull. 47 (2012) 432–437.

[27] P. Liang, Z. Yang, X. Chao, Z. Liu, Giant dielectric constant and good temperature stability in $Y_{2/3}Cu_3Ti_4O_{12}$ ceramics, J. Am. Ceram. Soc. 95 (2012) 2218–2225.

[28] W. Somphan, P. Thongbai, T. Yamwong, S. Maensiri, High Schottky barrier at grain boundaries observed in $Na_{1/2}Sm_{1/2}Cu_3Ti_4O_{12}$ ceramics, Mater. Res. Bull. 48 (2013) 4087–4092.

[29] L. Sun, Z. Wang, Y. Shi, E. Cao, Y. Zhang, H. Peng, L. Ju, Sol–gel synthesized pure $CaCu_3Ti_4O_{12}$ with very low dielectric loss and high dielectric constant, Ceram. Int. 41 (2015) 13486–13492.

[30] W. Wan, C. Liu, H. Sun, Z. Luo, W.X. Yuan, H. Wu, T. Qiu, Low-toxic gelcasting of giant dielectric-constant $CaCu_3Ti_4O_{12}$ ceramics from the molten salt powder, J. Eur. Ceram. Soc. 35 (2015) 3529–3534.

[31] S. Vangchangyia, E. Swatsitang, P. Thongbai, S. Pinitsoontorn, T. Yamwong, S. Maensiri, V. Amornkitbamrung, P. Chindaprasirt, Very low loss tangent and high dielectric permittivity in pure-$CaCu_3Ti_4O_{12}$ ceramics prepared by a modified sol-gel process, J. Am. Ceram. Soc. 95 (2012) 1497–1500.

[32] J. Boonlakhorn, P. Thongbai, B. Putasaeng, T. Yamwong, S. Maensiri, Very high-performance dielectric properties of $Ca_{1-3x/2}Yb_xCu_3Ti_4O_{12}$, ceramics 612 (2014) 103–109.

[33] R.D. Shannon, Revised effective ionic radii and systematic studies of interatomic distances in halides and chalcogenides, Acta Crystallogr. A 32 (1976) 751–767.

[34] P. Thongbai, T. Yamwong, S. Maensiri, V. Amornkitbamrung, P. Chindaprasirt, Improved dielectric and nonlinear electrical properties of fine-grained $CaCu_3Ti_4O_{12}$ ceramics prepared by a glycine-nitrate process, J. Am. Ceram. Soc. 97 (2014) 1785–1790.

[35] J. Jumpatam, N. Chanlek, M. Takesada, P. Thongbai, Giant dielectric behavior of monovalent cation/anion (Li^{+}, F^{-}) co-doped $CaCu_3Ti_4O_{12}$ ceramics, J. Am. Ceram. Soc. 103 (2020) 1871–1880.

[36] J. Jumpatam, W. Somphan, J. Boonlakhorn, B. Putasaeng, P. Kidkhunthod, P. Thongbai, S. Maensiri, Non-Ohmic properties and electrical responses of grains and grain boundaries of $Na_{1/2}Y_{1/2}Cu_3Ti_4O_{12}$ ceramics, J. Am. Ceram. Soc. 100 (2017) 157–166.

[37] K.T. Jacob, C. Shekhar, X. Li, G.M. Kale, Gibbs energy of formation of $CaCu_3Ti_4O_{12}$ and phase relations in the system CaO–CuO/Cu_2O–TiO_2, Acta Mater. 56 (2008) 4798–4803.

[38] S.Y. Lee, H.E. Kim, S.I. Yoo, Subsolidus phase relationship in the CaO–CuO–TiO_2 ternary system at 950°C in air, J. Am. Ceram. Soc. 97 (2014) 2416–2419.

[39] M. Li, Z. Shen, M. Nygren, A. Feteira, D.C. Sinclair, A.R. West, Origin(s) of the apparent high permittivity in $CaCu_3Ti_4O_{12}$ ceramics: clarification on the contributions from internal barrier layer capacitor and sample-electrode contact effects, J. Appl. Phys. 106 (2009), 104106.

[40] L. Sun, R. Zhang, Z. Wang, E. Cao, Y. Zhang, L. Ju, Microstructure and enhanced dielectric response in Mg doped $CaCu_3Ti_4O_{12}$ ceramics, J. Alloys Compd. 663 (2016) 345–350.

[41] P. Thongbai, J. Jumpatam, B. Putasaeng, T. Yamwong, S. Maensiri, The origin of giant dielectric relaxation and electrical responses of grains and grain boundaries of W-doped $CaCu_3Ti_4O_{12}$ ceramics, J. Appl. Phys. 112 (2012), 114115.

[42] J. Wu, C.W. Nan, Y. Lin, Y. Deng, Giant dielectric permittivity observed in Li and Ti doped NiO, Phys. Rev. Lett. 89 (2002), 217601.

[43] K. Meeporn, T. Yamwong, S. Pinitsoontorn, V. Amornkitbamrung, P. Thongbai, Grain size independence of giant dielectric permittivity of $CaCu_3Ti_{4-x}Sc_xO_{12}$ ceramics, Ceram. Int. 40 (2014) 15897–15906.

[44] J. Boonlakhorn, P. Kidkhunthod, B. Putasaeng, T. Yamwong, P. Thongbai, S. Maensiri, Giant Dielectric Behavior and Electrical Properties of $Ca_{1-3x/2}Lu_xCu_3Ti_4O_{12}$ Ceramics, vol. 120, 2015, pp. 89–95.

[45] L. Singh, B.C. Sin, I.W. Kim, K.D. Mandal, H. Chung, Y. Lee, J. Varela, A novel one-step flame synthesis method for tungsten-doped CCTO, J. Am. Ceram. Soc. 99 (2016) 27–34.

[46] L. Ni, X.M. Chen, Dielectric relaxations and formation mechanism of giant dielectric constant step in $CaCu_3Ti_4O_{12}$ ceramics Appl, Phys. Lett. 91 (2007), 122905.

[47] R. Kashyap, R.K. Mishra, O.P. Thakur, R.P. Tandon, Structural, dielectric properties and electrical conduction behaviour of Dy substituted $CaCu_3Ti_4O_{12}$ ceramics, Ceram. Int. 38 (2012) 6807–6813.